Available online at www.sciencedirect.com
SCIENCE DIRECT
Cement and Concrete Research 35 (2005) 431–437
CEMENT AND CONCRETE RESEARCH

Chlorellestadite in the preheater system of cement kilns as an indicator of HCl formation

Simon Jegou Saint-Jean[a,*], Ebbe Jøns[b], Niels Lundgaard[b], Staffan Hansen[a]

[a]*Materials Chemistry, Centre for Chemistry and Chemical Engineering, Lund University, P.O. Box 124, SE-221 00 Lund, Sweden*
[b]*F.L. Smidth A/S, Research and Development Laboratory, Vigerslev Allé 77, DK-2500 Valby, Copenhagen, Denmark*

Received 22 September 2003; accepted 17 May 2004

Abstract

The conditions leading to the formation of water-insoluble chlorellestadite, ideal formula (unit cell content) $Ca_{10}(SiO_4)_3(SO_4)_3Cl_2$, instead of water-soluble KCl and NaCl in Portland cement kiln systems were investigated by quantitative X-ray phase analysis of plant samples, preparation of pure chlorellestadite, and thermodynamic calculations. The results support the view that water-insoluble chloride is present as chlorellestadite. A reason for its occurrence could be poor contact between the hot kiln gases and lime-containing dust causing formation of gaseous HCl, which then produces chlorellestadite in contact with the hot meal in the preheater unit.

The structure model for synthetic chlorellestadite, used in the quantitative X-ray phase analysis, was refined by the full profile Rietveld method using the powder X-ray diffraction spectrum ($CuK_{\alpha 1}$). Crystal data: hexagonal, space group $P6_3/m$, $a = 9.6773(3)$ Å, $c = 6.8585(1)$ Å, $Z = 1$. A disordered S/Si distribution was observed.

Keywords: X-ray diffraction; Chloride; Cement manufacture; Modelling

1. Introduction

At present, use of industrial waste materials as alternative fuels in cement kilns is increasing. Some waste materials, such as PVC and chlorinated hydrocarbons, can increase the amount of Cl introduced in the kiln during the production of Portland cement clinker. Under unfavourable circumstances, some of the Cl normally present in the kiln atmosphere in the form of NaCl and KCl can be replaced by HCl, which can cause corrosion on the steel walls of the rotating furnace. The area of attack is usually in the transition zone of the kiln [1].

When hot kiln gases enter the preheater system and meet the hot meal, chemical reactions take place, which sometimes cause product buildup on the walls of the cyclones and riser ducts. Clogging of the tubes may lead to decreased clinker output and necessitate costly cleaning processes. It has been observed (Ebbe Jøns, private communication) that the preheater coatings may contain substantial amounts of Cl in water-insoluble form instead of the more common water-soluble KCl and NaCl. The water-insoluble, Cl-containing phase has been identified as chlorellestadite, an apatite-type structure with the ideal composition $Ca_{10}(SiO_4)_3(SO_4)_3Cl_2$. Different variants of ellestadite $Ca_{10}(SiO_4)_3(SO_4)_3X_2$ (X = OH, F, Cl) can be found in nature, e.g., at Crestmore, California, and The Chichibu Mine, Japan [2,3], as well as in kiln coatings in the cement industry [4,5]. In the present paper, we investigate the possibility of using quantitative Rietveld analysis of preheater deposits containing chlorellestadite as a means of detecting the presence of HCl gas in cement kilns.

2. Experimental

2.1. Plant samples

Seven samples were obtained from different cement plants and regions of the kiln system. Samples 1, 2, and 3 are hot meal collected during a full-scale plant test. Number 1 is sampled before the test started, whereas Samples 2 and 3 were collected at different times during a period when

* Corresponding author. Tel.: +46-46-222-83-32; fax: +46-46-222-40-12.
E-mail address: simon.jegou_saint-jean@materialkemi.lth.se (S. Jegou Saint-Jean).

0008-8846/$ – see front matter © 2004 Elsevier Ltd. All rights reserved.
doi:10.1016/j.cemconres.2004.05.028

$CaSO_4$ and CaF_2 was added to the kiln feed. Sample 4 is a dust sample from a riser duct and Sample 5 is the same sample after slurrying in water. Sample 6 is the coating coming from a riser pipe and Sample 7 is the dust from the fifth stage of a preheating tower. Sample 7 was treated with glycol [6] to remove the free lime. The samples were analysed for their chlorine, sulphur, and potassium contents. Samples 5, 6, and 7 were selected for further analysis by X-ray powder diffraction to identify and quantify the phases containing water-insoluble Cl.

The total sulphur content was determined by means of a LECO CS-300 analyser, the chlorine content by chloride potentiometric titration, and the potassium by X-ray fluorescence using a Philips PW 1606 X-ray spectrometer. The X-ray diffraction data were collected for 2 h with a Philips PW 1800 diffractometer using $CuK_{\alpha 1}$ radiation (from $2\theta = 5$ to 65° and a step size of 0.02°).

2.2. Laboratory samples

Chlorellestadite, with the ideal formula $Ca_{10}(SiO_4)_3(SO_4)_3Cl_2$, was prepared by heating stoichiometric amounts of CaO, SiO_2, and $CaSO_4$ with $CaCl_2$ in excess. The starting materials used were prepared by preheating the following for 1 h: $CaCO_3$ (Merck, p.a.) at 1000 °C; amorphous silica $SiO_2 \cdot 0.18H_2O$ (Kebo, purum) and $CaSO_4 \cdot 2H_2O$ (Merck, p.a.) at 600 °C; and finally $CaCl_2 \cdot 2H_2O$ (Riedel-de Haën, p.a.) at 400 °C. After grinding in acetone (Merck, p.a.) and drying, the mixture was discharged in an alumina boat and heated at 1000 °C in a tube furnace for 4 h. Both quenching and slow cooling were tried and gave the same results. The samples were washed with water to remove excess $CaCl_2$ and analysed by scanning electron microscopy and X-ray fluorescence. The total sulphur content was determined by means of a LECO CS-300 analyser and the chlorine content by chloride potentiometric titration.

X-ray diffraction analysis was performed on samples of chlorellestadite powder mounted on Scotch tape using a Guinier focusing camera equipped with an imaging plate (Huber Imaging Plate Guinier Camera 670). Data were collected for 32 000 s (≈ 9 h), using $CuK_{\alpha 1}$ radiation from $2\theta = 8$ to 100°, with a 2θ step of 0.005°. Single-crystal X-ray diffraction analysis of needle-shaped crystals was also tried but the weak intensity of the observed diffraction spots did not allow the collection of reliable data.

2.3. Thermodynamic calculations

The HSC program [7] was used to simulate the evolution of the kiln atmosphere upon cooling from the burning temperature down to 1000 °C, although the calculation is actually performed in the other direction, starting at 1000 °C and then increasing the temperature. The principle of the simulation is to monitor the evolution with temperature of the amount of various species (in the gaseous and condensed states) enclosed in a box of varying volume at a fixed pressure of 1 atm. The simulations must be treated as illustrative because of the oversimplification of the thermodynamic model. The model consists of pure solid phases, an ideal melt, and an ideal gas phase. At each step of temperature, the program calculates the multiphase equilibrium compositions by using the Gibbs energy minimization method. Simulation 1 represents a case with sufficient contact between the kiln gases and CaO-containing dust, whereas in Simulation 2 the contact to CaO dust is limited (the amount of CaO is set to zero in the starting conditions). Starting conditions for the simulations, using data collected during production of mineralised clinker, together with a list of species and quantities used for the calculations, are given in Table 1.

Table 1
Starting conditions and raw materials in the thermodynamic simulations

Simulation 1: sufficient contact with CaO dust		Simulation 2: insufficient contact with CaO dust	
Raw materials (mol)		*Raw materials (mol)*	
CO_2(g)	16.300	CO_2(g)	16.300
H_2O(g)	5.130	H_2O(g)	5.130
O_2(g)	2.000	O_2(g)	2.000
N_2(g)	80.000	N_2(g)	80.000
CaO(s)	17.000	HCl(g)	0.610
$CaCl_2$(l)	0.305	SO_2(g)	1.000
$CaSO_4$(l)	1.750	$CaSO_4$(l)	1.750
K_2CO_3(l)	0.831	K_2CO_3(l)	0.831
Na_2CO_3 (l)	0.291	Na_2CO_3 (l)	0.291

Temperature, 1000 °C; pressure, 1 atm.
The chemical system consists of 23 species in different physical states. Gaseous: CO, CO_2, HCl, H_2O, KCl, KOH, NaCl, NaOH, Na_2SO_4, K_2SO_4, O_2, SO_2, SO_3 and N_2. Liquid: $CaCl_2$, KCl, NaCl, $CaSO_4$, K_2CO_3, K_2SO_4, Na_2CO_3 and Na_2SO_4. Solid: CaO.

3. Results and discussion

3.1. Chemical analysis of plant samples

In all the plant samples analysed by X-ray powder diffraction, the chlorellestadite phase was detected. The partial chemical analysis of the plant samples is presented in Table 2.

Comparison of the reference hot meal (Sample 1) and the corresponding test hot meals (Samples 2 and 3) showed that the contents of potassium and chloride decrease (40% lower) during the test, whereas the sulphur content increases. It is further seen that the nature of chloride in the hot meal changes from highly water soluble to sparingly water soluble. There is little difference between the two test samples. It can be concluded that the relative amount of water-insoluble chloride is a parameter that is highly sensitive to changes in the clinker burning process.

As could be expected, the contact with water decreased the amount of water-soluble Cl in Sample 5 as compared to Sample 4.

Table 2
Partial chemical analysis of the plant samples

	Sample (wt.%)						
	1	2	3	4	5	6	7
K_2O	2.38	1.63	1.65			2.77	2.11
S total	0.61	1.10	1.50				
SO_3				4.00	3.90	6.49	
Cl total	0.63	0.37	0.35	0.22	0.17	3.39	0.85
Cl water soluble	0.54	0.22	0.20	0.11	0.03	1.73	0.57
Expected chlorellestadite[a]	1.3	2.2	2.2	1.6	2.0	24.3	8.5
Expected KCl[b]	1.0	0.42	0.38	0.21	0.06	3.30	1.1

The origin of the different samples is described in the Experimental section.
[a] Values calculated taking chlorellestadite (Cl = 6.84 wt.%) as the only Cl-containing, water-insoluble phase. For sample 7, the calculated value is corrected for the free lime content (52 wt.%).
[b] Assuming KCl to be the only water-soluble, Cl containing phase.

3.2. Structural analysis of laboratory samples

The washed samples consisted of pure chlorellestadite in the form of a very fine white powder containing 5-μm crystal plates and a few needle-shaped crystals (3 × 100 μm) grown from the $CaCl_2$ flux. The composition, as determined by X-ray fluorescence and chemical analyses (Table 3), was $Ca_{9.99}(SiO_4)_{3.17}(SO_4)_{2.85}Cl_{1.85}$. This confirms the general stoichiometry expected for chlorellestadite, i.e., $Ca_{10}(SiO_4)_3(SO_4)_3Cl_2$.

Rietveld refinements based on powder X-ray data were carried out using the program WINPOW [8], a local Windows version of the Rietveld analysis program LHPM 1 by Hill and Howard [9]. The hexagonal chlorapatite structure [10] was chosen as starting model. The pseudo-Voigt function was used for the simulation of the peak shape and the peaks were corrected for asymmetry effects. The background was modelled by using the Chebyshev function. Details of the refinement process and results are given in Tables 4 and 5, and the final Rietveld plot of chlorellestadite is shown in Fig. 1.

Like most of the apatite-type structures, the synthesized chlorellestadite was found to crystallize in the hexagonal system and space group $P6_3/m$. Its atomic structure is similar to that of chlorapatite $Ca_{10}(PO_4)_6Cl_2$ with substitution of one silicon and one sulphur for two phosphorus. The calcium atoms are located in two distinct crystallographic sites: the Ca(1) atoms in special Wyckoff position 4(f) at $z \approx 0$ and $z \approx 1/2$ forming columns parallel to the c axis at x = 1/3, y = 2/3 and at x = 2/3, y = 1/3; and Ca(2) atoms in special position 6(h) around the origin of the unit cell forming two triangular arrays of Ca(2) atoms on the mirror planes at $z = 1/4$ and $z = 3/4$, thus forming columns of Ca octahedra sharing faces along the c axis. The special position 6h occupied by P in the chlorapatite structure is here occupied by 50% S and 50% Si, leading to a random distribution of SiO_4– and SO_4–tetrahedra in the structure, with a refined average bond length (Si,S)–O = 1.55(3) Å, which is the same as the average value 1.55 Å calculated from the typical observed values: Si–O = 1.63 Å in silicates [11] and S–O = 1.47 Å in sulphates [12]. An ordering of the Si and S atoms in space group $P6_3/m$ is made possible only by a doubling of the unit cell in the a or b direction, which has not been detected here and, to our knowledge, has not been reported so far. The Cl ions lie in the special position

Table 3
Chemical composition (wt.%) of synthetic chlorellestadite

	CaO	SiO_2	SO_3	Cl
This study[a]	53.46	18.09	21.95[b]	6.27
Ref. [5]	53.915	17.635	22.185	6.075

[a] The impurities, representing a total amount of 0.13 wt.%, are neglected here.
[b] The determination of the total sulphur amount using a LECO device gives almost the same result as with X-ray fluorescence (8.73 compared to 8.79 wt.%).

Table 4
Rietveld refinement parameters and residuals for the synthetic chlorellestadite

a (Å)	9.6773(3)
c (Å)	6.8585(1)
V (Å^3)	556.25(4)
Unit cell content	$Ca_{10}(SiO_4)_3(SO_4)_3Cl_2$
Space group	$P6_3/m$
R_p (%)	14.31
R_{wp} (%)	14.59
GOF (%)	5.48
R_B (%)	7.58
Number of Bragg reflections	251
Number of parameters refined	36
2θ range	12°–98°
2θ step	0.01°

$$R_p = \frac{\sum_i |Y_i - Y_{c,i}|}{\sum_i Y_i}, \quad R_{wp} = \sqrt{\frac{\sum_i w_i (Y_i - Y_{c,i})^2}{\sum_i w_i (Y_i)^2}},$$

$$\mathrm{GOF} = \sum_i w_i \frac{(Y_i - Y_{c,i})^2}{n-p}, \quad R_B = \sum_k |Y_i - Y_{c,i}| \Big/ \sum_k I_{ko}$$

where Y_i is the observed intensity at point i and $Y_{c,i}$ the calculated one, R_p the profile residual, R_{wp} the weighted residual, GOF the goodness of fit (n is the number of observations and p the number of refined parameters) and R_B the residual formed from the Bragg intensities.

Table 5
Final coordinates, occupancies and isotropic temperature factor coefficients for the synthetic chlorellestadite as derived from the Rietveld refinements

	x	y	z	g	B (Å^2)
Ca(1)	1/3	2/3	−0.0051(5)	1/3	2.0(1)
Ca(2)	0.2592(3)	−0.0045(3)	1/4	1/2	2.1(1)
Si	0.4073(4)	0.3738(3)	1/4	1/4	1.3(1)
S	0.4073(4)	0.3738(3)	1/4	1/4	1.3(1)
O(1)	0.3395(7)	0.4941(7)	1/4	1/2	2.1(1)
O(2)	0.5859(7)	0.4716(7)	1/4	1/2	2.1(1)
O(3)	0.3444(5)	0.2625(5)	0.0673(6)	1	2.1(1)
Cl	0	0	0.451(2)	1/6	6.9(3)

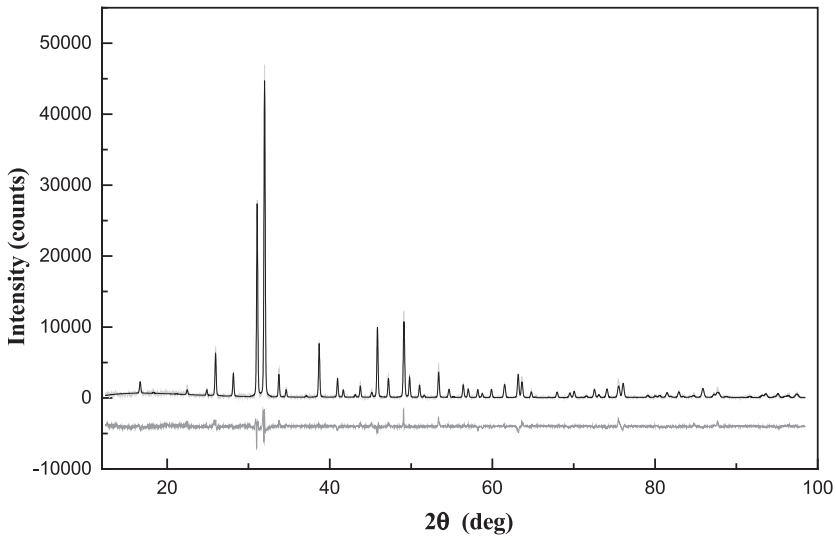

Fig. 1. The final Rietveld plot of the synthetic chlorellestadite. The upper trace illustrates the observed data and the lower trace is a plot of the difference between the observed and calculated intensities.

4(e) at (0,0,1/2-Δz), i.e., displaced by Δz from the ideal special position (2b) at (0,0,1/2). Their site occupancy was set statistically to 50% in the refinement to counter the doubling effect of the mirror planes at $z = 1/4$ and $z = 3/4$. This refined structure of the chlorellestadite was used for the quantitative X-ray diffraction analysis of the plant samples 5, 6, 7.

3.3. Quantitative phase analysis of plant samples

The quantification of the chlorellestadite and the other crystalline phases composing the plant samples was achieved by using the Siroquant program [13], refining the instrumental and profile parameters of each phase. The program calculates, for each refinement cycle, an estimate of the abundance of each phase, using the formula:

$$W_P = \frac{S_P(ZMV)_P}{\tau_P}\left(\sum_{j=1}^{N}\frac{S_j(ZMV)_j}{\tau_j}\right)^{-1}$$

where W_P is the mass fraction of phase P, S the Rietveld scale factor, Z the number of formula units per unit cell, M the mass of the formula unit, V the unit cell volume and τ_j the absorption contrast factor of phase j. The content of chlorellestadite calculated from the chemical analyses of Cl (Table 2), assuming the ideal composition $Ca_{10}(SiO_4)_3(SO_4)_3Cl_2$, and the Siroquant results (Table 6) are not in good agreement, although they corroborate the fact that the water-insoluble chlorine-containing crystalline phase is essentially chlorellestadite.

The X-ray results indicate a content of chlorellestadite 2.3 to 3.0 times higher than the calculated content. A lower content of Cl than the ideal one (6.84 wt.%) in the apatite-type phase will strongly affect the level calculated from the chemical analysis of plant samples. This can be the result of substitutions of F^- and OH^- for Cl^- in the chlorellestadite structure, as well as other crystal chemical mechanisms causing a Cl deficiency. Substitutions of F^- and OH^- for Cl^- in the equal proportions 1/3:1/3:1/3 or of OH^- only in the proportions 2/3:1/3, will both lead to 2.33 wt.% Cl in chlorellestadite. In Sample 6 this will lead to an expected content of substituted chlorellestadite in the plant sample almost three times higher (71.24 wt.%) than with stoichiometric chlorellestadite, in better concordance with the values obtained with the quantitative XRD analysis (63.9 wt.%). The X-ray quantification, on the other hand, could be affected by a high percentage of nondiffracting amorphous phases, which is generally not observed in the cement production.

A comparison of the unit cell parameters of different ellestadites is made in Table 7. The chlorellestadite in the plant samples 5–7 and natural ellestadite from Crestmore [2] are similar, whereas synthesized chlorellestadite (this

Table 6
Quantitative phase analysis of the plant samples using powder X-ray diffraction

Sample 5	wt.%	Sample 6	wt.%	Sample 7	wt.%
Chlorellestadite	6.0(6)	Chlorellestadite	63.9(4)	Chlorellestadite	19.1(5)
KCl	–	KCl	1.9(1)	KCl	0.5(1)
Quartz	4.5(3)	–		Quartz	30.0(5)
Calcite	70.4(6)	–		Calcite	4.5(3)
–		Anhydrite	2.2(2)	Anhydrite	6.3(3)
–		Periclase	1.5(3)	Periclase	19.1(4)
Portlandite	19.1(3)	Mayenite	7.4(4)	β-C_2S	10.7(6)
		Lime	23.2(3)	Hematite	4.7(2)
				Muscovite	4.0(8)
				Microcline	1.1(7)
χ^2	9.57		10.40		10.69

$$\chi^2 = \left(\sum \frac{(Y_O - Y_C)^2}{Y_O(NO - NV)}\right)^{1/2}$$

where (NO – NV) is the degree of freedom.

Table 7
Refined unit cell parameters of chlorellestadite in the plant samples, a natural ellestadite and synthetic chlorellestadites

Lattice parameters	a (Å)	c (Å)	V (Å^3)	c/a
Sample 5	9.520	6.918	543.0	0.7266
Sample 6	9.535	6.923	544.3	0.7261
Sample 7	9.553	6.917	546.7	0.7241
Mineral [2]	9.530	6.914	543.8	0.7255
Synthetic, this study	9.677	6.858	556.3	0.7087
Synthetic [5]	9.688	6.849	556.7	0.7071

study and Ref. [5]), form a separate group with larger unit cells. This is another indication of substitution with smaller anions or other type of chlorine deficiency.

When the synthetic chlorellestadite is used as a starting model in the quantification of the plant samples, the refinement result is a smaller unit cell, which is coupled to the splitting of the major doublet peak in the diffraction pattern into a triplet peak (cf. Figs. 1 and 2a). Stoichiometric chlorellestadite or Cl-deficient chlorellestadite [14], does not produce the correct intensity distribution for the triplet. This can be achieved, though, by using a mixed anion apatite model [15] with (i) OH, F and Cl occupancies set to 1/3 at their respective special atomic positions: (0, 0, 0.189), (0, 0, 1/4) and (0, 0, 0.407) or (ii) the equivalent model with 2/3 OH and 1/3 Cl. The calculated pattern (Fig. 2b) gives an almost perfect fit with the observed profiles of the plant samples (Fig. 2c), but without significant changes in the quantification results. The clear difference in the intensity distribution of the main peaks between the chlorellestadite (Fig. 2a) and the substituted models (Fig. 2b) thus confirms that the chlorellestadite formed in kiln coatings deviates from the ideal composition as a result of ionic substitutions, rather than Cl deficiency.

The expected content of KCl (Table 2), assuming this to be the only water-soluble compound formed, is higher than the one observed by X-ray analysis (Table 6), although the trend observed when comparing Samples 5–7 is consistent. This indicates a systematic difference between the two approaches and it should be noticed that the observed levels (0–2 wt.%) are not far from the detection limit of the X-ray method. No NaCl phase could be unambiguously detected by X-rays and this could account for the missing soluble chloride.

3.4. Thermodynamic calculations

Most of the volatile components present in the riser duct come from the burning zone of the kiln. The main components in the gas phase in the burning zone are $SO_2(g)$, KCl(g) and NaCl(g), whereas the content of HCl(g) is normally very low. The gas phase components will start to condense as the temperature decreases and the first condensed components are calcium alkali sulphates. This can schematically lead to two types of reaction, here modelled as the extent of contact with lime-containing dust.

Gas phase reaction:

$$SO_2(g) + 2KCl(g) + H_2O(g) + 1/2O_2(g) \leftrightharpoons K_2SO_4(l) + 2HCl(g)$$

Dust contact reaction:

$$SO_2(g) + 2KCl(g) + CaO(s) + 1/2O_2(g) \leftrightharpoons CaSO_4(s) + 2KCl(g)$$

The gas phase reaction produces HCl from KCl, whereas in the dust reaction, the KCl does not react. The

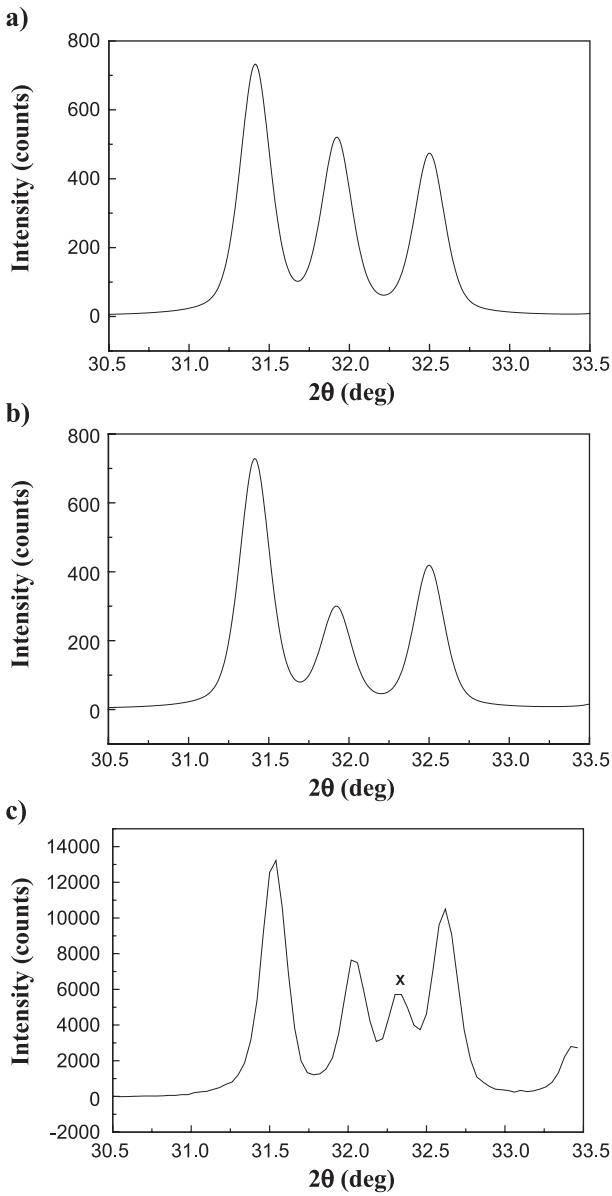

Fig. 2. (a) Plot of the main peaks of the chlorellestadite diffraction pattern and (b) the (OH, Cl, F)-ellestadite diffraction pattern. Both were calculated using the refined cell parameters $a = 9.535$ Å and $c = 6.923$ Å, obtained from the quantitative X-ray analysis of Sample 6. The (OH, Cl)-ellestadite pattern is similar to (b). (c) Plot of the main peaks of chlorellestadite in Sample 6 (the peak marked with a cross indicates the lime phase).

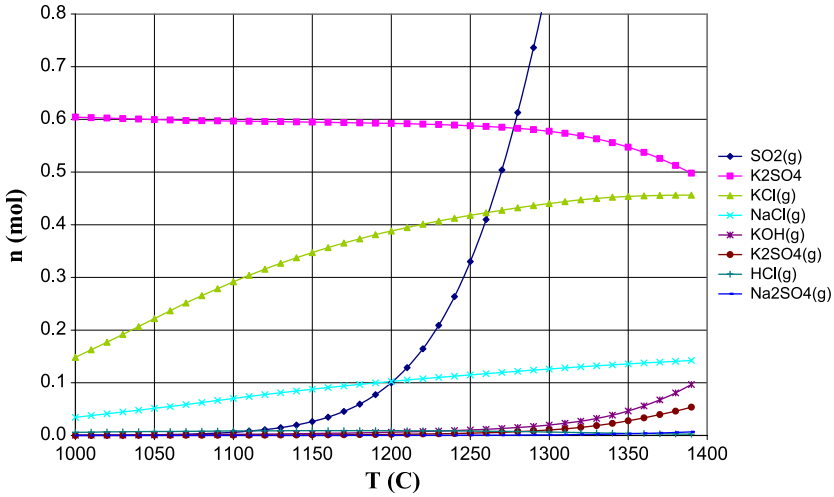

Fig. 3. Thermodynamic calculations simulating the reactions on cooling with sufficient contact with lime-containing dust (Simulation 1, Table 1).

reactions are illustrated by two reactor calculations, one with sufficient contact with lime-containing dust (Fig. 3) and one with insufficient contact with CaO dust (Fig. 4). In Fig. 3, it is seen that $SO_2(g)$ disappears from the gas phase without significant formation of HCl(g). Consequently, it will not be possible to measure significant amounts of $SO_2(g)$ in the kiln inlet in this situation. In the case of the calculation without sufficient contact with CaO-containing dust (Fig. 4), it is seen that there is a discontinuity in the $SO_2(g)$ concentration at around 1225 °C, where all lime has reacted. Further decrease in temperature will lead to the formation of alkali sulphates and HCl(g). It will, in this case, be possible to measure $SO_2(g)$ in the kiln inlet. The $SO_2(g)$ concentration in the kiln inlet can be as high as 5000 ppm. Half of the chloride reaching the kiln inlet is in the form of HCl(g). The HCl(g) concentration can be reduced by better gas solid contact in the kiln, i.e., reabsorption.

The reaction $CaO(s) + 2HCl(g) \rightarrow CaCl_2(l) + H_2O(g)$ becomes more spontaneous with decreasing temperature, and after the formation of calcium chloride the mixture (CaO, SiO_2, $CaSO_4$, $CaCl_2$), which readily forms chlorellestadite at 1000 °C in the laboratory preparations, is also present close to the kiln inlet. This strongly suggests that chlorellestadite is a good indicator for the presence of gaseous HCl.

4. Conclusions

- Quantitative phase analysis based on powder X-ray diffraction data of materials in cement kilns can be used to verify the presence of chlorellestadite, a marker phase that indicates the formation of HCl in the hot atmosphere.
- The quantification of chlorellestadite by using the contents of water soluble/insoluble chloride is sensitive to the actual chloride content in the crystals.

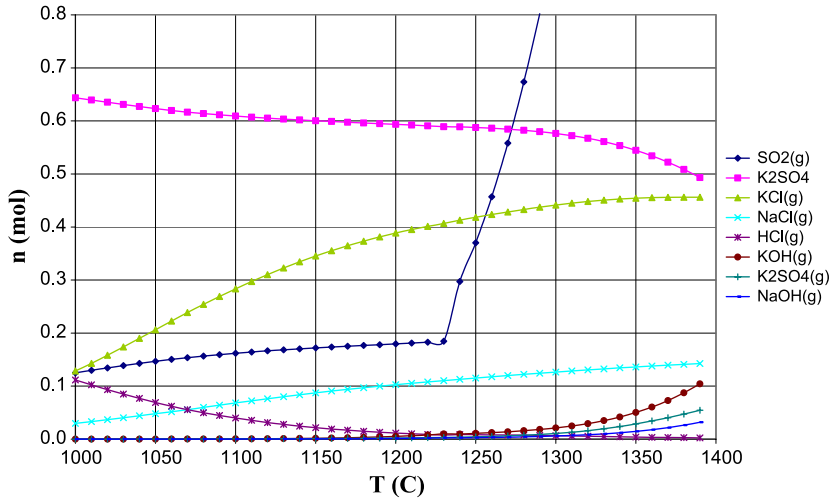

Fig. 4. Thermodynamic calculations simulating the reactions on cooling without sufficient contact with lime-containing dust (Simulation 2, Table 1).

– The ambient conditions and crystal chemical mechanisms affecting the chemical composition of synthetic and plant chlorellestadites need further investigation.

References

[1] E.S. Jøns, M.J.L. Østergård, Investigations into shell corrosion of rotary cement kilns, Zem.-Kalk-Gips 52 (1999) 68–79.
[2] R.C. Rouse, P.J. Dunn, A contribution to the crystal chemistry of ellestadite and the silicate sulfate apatites, Am. Mineral. 67 (1982) 90–96.
[3] K. Harada, K. Nagashima, K. Nakao, A. Kato, Hydroxylellestadite, a new apatite from Chichibu mine, Saitama prefecture, Japan, Am. Mineral. 56 (1971) 1507–1518.
[4] Y. Pliego-Cuervo, F.P. Glasser, Phase relations and crystal chemistry of apatite and silicocarnotite solid solutions, Cem. Concr. Res. 8 (1978) 519–524.
[5] M. Chen, Y. Fang, The chemical composition and crystal parameters of calcium chlorosulfatosilicate, Cem. Concr. Res. 19 (1989) 184–188.
[6] M.P. Javellana, I. Jawed, Extraction of free lime in Portland cement and clinker by ethylene glycol, Cem. Concr. Res. 12 (1982) 399–403.
[7] HSC Chemistry for Windows 2.0, Outokumpu Research, P.O. Box 60, FIN-28101 Pori, Finland, 1994.
[8] Ståhl, K., WINPOW, program for Rietveld refinement, Technical University of Denmark, Lyngby, 2002.
[9] R.J. Hill, C.J. Howard, Australian Atomic Energy Commission (now ANSTO), Report M112, Lucas Heights Research Laboratories, New South Wales, Australia, 1986.
[10] P.E. Mackie, J.C. Elliot, R.A. Young, Monoclinic structure of synthetic $Ca_5(PO_4)_3Cl$, chlorapatite, Acta Crystallogr. B 28 (1972) 1840–1848.
[11] J.V. Smith, S.W. Baily, Second review of Al–O and Si–O tetrahedral distances, Acta Crystallogr. 16 (1963) 801–811.
[12] B.J. Wuench, Sulfur, 16-A Crystal chemistry, in: K.H. Wedepohl (Ed.), Handbook of Geochemistry, Vol. II/2, Springer-Verlag, Berlin, pp. 16A1–16A19, 1970.
[13] J.C. Taylor, Computer programs for standardless quantitative analysis of minerals using the full powder diffraction profile, Powder Diffr. 6 (1991) 2–9.
[14] S. Jegou Saint-Jean, S. Hansen, Solid State Sci., submitted for publication.
[15] K. Sudarsanan, R.A. Young, Structural interactions of F, Cl and OH in apatites, Acta Crystallogr. B 34 (1978) 1401–1407.